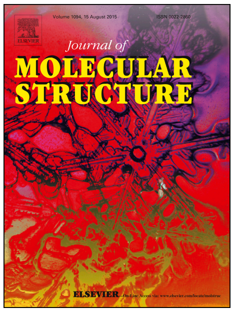

Benzo[c][1,2,5]selenadiazole organoselenium derivatives: Synthesis, X-ray, DFT, Fukui analysis and electrochemical behavior

Halima Ouahine, Ali Hasnaoui, Ismail Hdoufane, Rachid Idouhli, Abdessalam Abouelfida, Mustapha Ait Ali, Larbi El Firdoussi

PII: S0022-2860(19)31005-1

DOI: https://doi.org/10.1016/j.molstruc.2019.126914

Reference: MOLSTR 126914

To appear in: *Journal of Molecular Structure*

Received Date: 23 May 2019

Revised Date: 6 August 2019

Accepted Date: 8 August 2019

Please cite this article as: H. Ouahine, A. Hasnaoui, I. Hdoufane, R. Idouhli, A. Abouelfida, M.A. Ali, L. El Firdoussi, Benzo[c][1,2,5]selenadiazole organoselenium derivatives: Synthesis, X-ray, DFT, Fukui analysis and electrochemical behavior, *Journal of Molecular Structure* (2019), doi: https://doi.org/10.1016/j.molstruc.2019.126914.

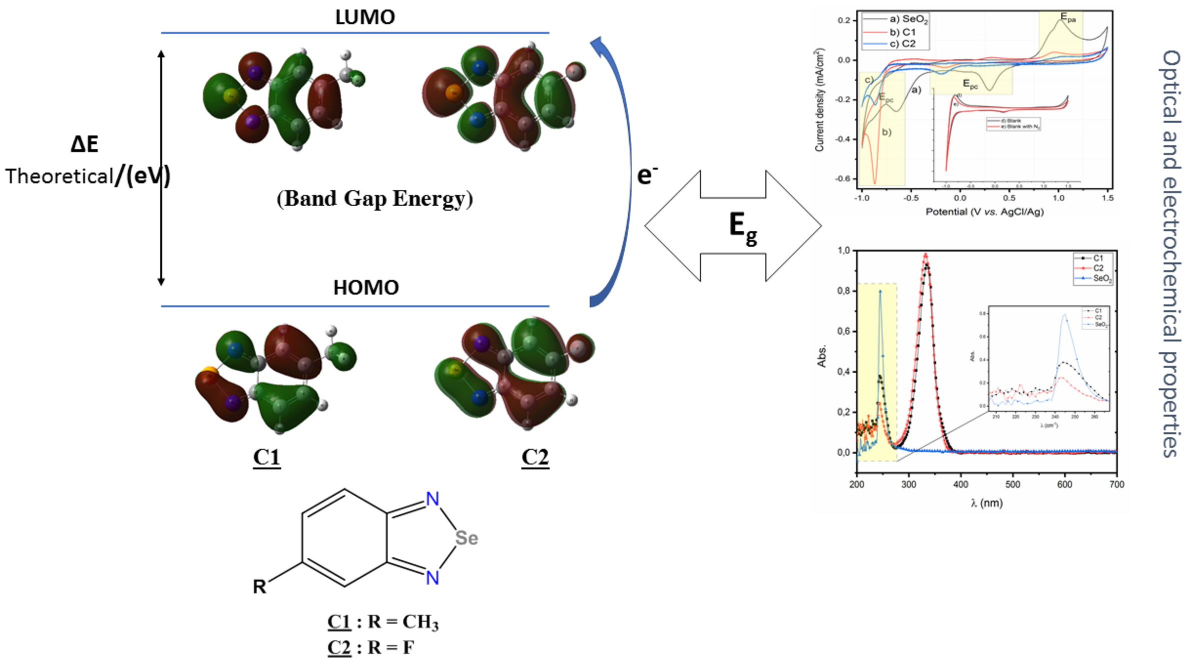
LUMO
ΔE
Theoretical/(eV)
(Band Gap Energy)
HOMO
e-
E_g
C1
C2
R
N
Se
N
C1 : R = CH3
C2 : R = F
a) SeO2
b) C1
c) C2
E_pa
E_pc
Current density (mA/cm2)
Potential (V vs. AgCl/Ag)
d) Blank
e) Blank with N2
Abs.
λ (nm)
C1
C2
SeO2
Optical and electrochemical properties

Benzo[c][1,2,5]selenadiazole organoselenium derivatives: Synthesis, X-ray, DFT, Fukui analysis and electrochemical behavior

Halima Ouahine [a], Ali Hasnaoui [a], Ismail Hdoufane [b], Rachid Idouhli [c], Abdessalam Abouelfida [c], Mustapha Ait Ali [a] and Larbi El Firdoussi [a]

[a] *Equipe de Chimie de Coordination et Catalyse, Université Cadi Ayyad, Faculté des Sciences Semlalia, BP 2390, Marrakech,Morocco.*

[b] *Laboratoire de Chimie Moléculaire, Université Cadi Ayyad, Faculté des Sciences Semlalia, BP 2390, Marrakech, Morocco.*

[c] *Physical-Chemistry of Materials and Environment Laboratory, Faculty of Sciences Semlalia, Cadi Ayyad University, Marrakech, Morocco.*

ABSTRACT

Organo-selenium compounds are of a broad spectrum of potential technical applications. To date, many efforts have been devoted to develop their chemistry. In this context, two benzo[c][1,2,5]selenadiazole compounds have been synthesized and characterized by ^{1}H NMR, ^{13}C NMR, ^{19}F NMR, MS and UV-Vis spectroscopic techniques. Both structures were confirmed using single-crystal X-ray diffraction analysis. Each compound crystallizes in monoclinic systems, space group $P2_1/c$ forming dimeric units due to the intermolecular Se···N interactions. The dimmers are further linked by weak π··π stacking interactions between 1,2,5-selenadiazole and the six-membered aromatic rings. The electrochemical behavior of the compounds has been investigated by cyclic voltammetry. Additionally, the structural geometrical parameters, vibrational, electronic transition, Fukui analysis and redox properties of the molecules have been rationalized by DFT and TD-DFT methods using B3LYP level of theory in conjunction with 6-311G(d,p) basis set implemented in Gaussian 09 program. As a result, an excellent correlation between the electronic transitions and the electrochemical behavior was found.

Keywords
Organo-selenium; X-ray; DFT; Fukui indices; Cyclic voltammetry; Optical properties.

*** Corresponding authors:**
Prof. Larbi El Firdoussi: (elfirdoussi@uca.ac.ma)

1. Introduction

Over the last few years, there has been an increasing interest in organo-selenium compounds chemistry [1–4], mainly due to their importance as reagents and intermediates in organic synthesis and asymmetric transformations, especially as excellent selective reagents for the allylic oxidation [5,6]. Apart from this, organo-selenium compounds have fascinating pharmacological activities; they act as antioxidants, antitumor, anti-inflammatory, antifungal, antibacterial and antiviral agent [6–11]. Furthermore, selenium is a micro nutriment naturally present in several redox active enzymes including glutathione peroxidase [12]. In addition, selenium compounds are used in xerography and synthesis of conducting materials and semiconductors [13,14].

In chemistry, selenium is known to easily take part in redox reactions involving one or two electron transitions. It should be noticed that organoselenides are considered as toxic and malodorous compounds [15]. Nevertheless, selenaheterocycles are weakly volatile and their toxicity is low [16]. Besides, it has been reported that several selenoxides are used as an effective catalyst for the bromination of organic substrates in presence of sodium bromide and hydrogen peroxide [17]. Also, organoselenides catalyze the allylic halogenation of alkenes and α-halogenation of ketones in presence of N-halo-succinimides [18]. Moreover, electrochemical procedure has been employed as an effective and convenient method because of its high selectivity in organic chemistry such as the synthesis of α-bromo alkyl aryl ketones [19]. Recently, we have been performed the cyclic voltammetry to investigate the redox behavior of a metal complex [20]. Herein, we study the chemistry of organoselenium compounds as important substructures in a broad range of natural and designed products.

Therefore, in view to prepare organic compounds that could be valuable for the oxidation of natural molecules, we have used the cyclic voltammetry (CV) [21] as inexpensive, selective and sensitive electrochemical technique in order to investigate the redox behavior of these compounds. In the current work, we report the results of our study dedicated to two organo-selenium derivatives: 5-methyl-benzo[c][1,2,5]selenadiazole (**C1**) [22] and 5-fluoro-benzo[c][1,2,5]selenadiazole (**C2**). The general procedure of the synthetic path is shown in **Scheme 1**. Moreover, structural parameters of the titled compounds were computed by theoretical studies using density functional theory (DFT) and time dependent density functional theory (TD-DFT) methods. Finally, optical and electrochemical properties using CV technique of both samples were investigated in order to confirm the chemical stability as well.

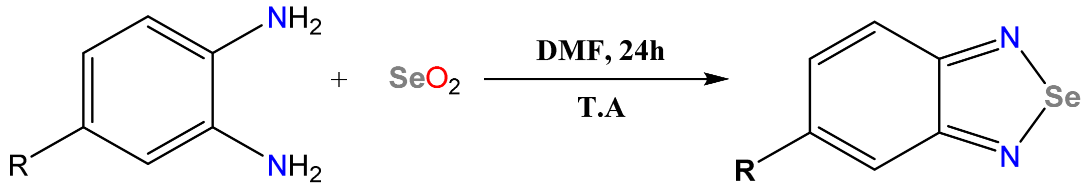

1 : R = CH_3
2 : R = F

Scheme 1. synthesis of benzo[c][1,2,5]selenadiazole derivatives

2. Experimental

2.1. Material and methods

4-methyl-o-phenylenediamine (**1**), 4-fluoro-o-phenylenediamine (**2**) selenium dioxide (**SeO_2**) and N,N-dimethylformamide were purchased from sigma Aldrich. Melting point was measured with Kofler heating bench. NMR spectra was recorded in $CDCl_3$ using a Bruker Avance 300 MHz spectrometer. Chemical shifts are expressed in ppm relative to external TMS. GC parameters for capillary columns TG-5MS (30 m x 0.25 mm): injector 230 °C; detector

200 °C; oven 40 °C for 2 min then 40 °C min^{-1} until 280 °C for 12 min; column pressure 42.9 kPa. Gas flow 20 mL min^{-1}. For MS detection, the ionization was performed on an ISQ LT single quadruple mass spectrometer in positive EI modes using a mass scan range of 50 to 400 Da.

2.2. Synthesis and crystallization

*2.2.1 5-methyl--benzo[c][1,2,5]Selenadiazole (**C1**).*

5-methyl-benzo[c][1,2,5]Selenadiazole has been prepared by the condensation of 4-methyl-o-phenylenediamine and selenium dioxide in N,N-dimethylformamide as described earlier in our previous work [22].

$C_7H_6N_2Se$ colorless. m/z =197.8[M]+ (**Fig. S4**). Mp=78 °C (from $CHCl_3$). ^1H NMR (300 MHz, $CDCl_3$, ppm): 2.4 (3H, s), 7.2 (1H, m), 7.5 (1H, m), 7.65 (CH, m). $^{13}C\{^1H\}$ NMR

(75 MHz, $CDCl_3$, ppm): 25.9 (CH_3), 126.3 (CH), 127.6 (CH), 137.7 (CH), 145.1 (Cq), 164.8 (Cq), 166.0 (Cq) (see **Fig. S2**).

*2.2.2 5-fluoro-benzo[c][1,2,5]Selenadiazole (**C2**).*

0.09 g (0.71 mmol) of 4-fluoro-o-phenylenediamine and 0.079 g (0.71 mmol) of **SeO_2** were dissolved in 5 mL of N,N-dimethylformamide. After stirring for 24 h at room temperature. The reaction mixture was diluted with 30 mL of water and extracted 3 times with 20 mL of ethyl acetate. The organic phases were dried over $MgSO_4$ and evaporated under reduced pressure. Pure product was isolated by column chromatography on silica gel using hexane/ethyl acetate (90/10) as eluent (yield: 84%). Yellowish crystals were obtained by crystallization from chloroform.

$C_6H_3FN_2Se$ color yellowish. m/z = 201.06 $[M\text{-}F]^+$ (**Fig. S4**). ^1H NMR (300 MHz. $CDCl_3$, ppm) 7.3 (1H, m), 7.4 (1H, Dd, J= 9.3, 2.4 Hz), 7.8 (1H, Dd, J=9.6, 5.7 Hz). $^{13}C\{^1H\}$ NMR (75 MHz, $CDCl_3$, ppm): 105.8 (CH, d, $^2J_{C\text{-}F}$=22.5 Hz), 122.0 (CH, d, $^2J_{C\text{-}F}$=30.0 Hz), 124.1 (CH, d, $^3J_{C\text{-}F}$=11 Hz), 158.0 (C_q, s) , 162.2 (C_q, d, $^3J_{Cq\text{-}F}$= 14 Hz), 164.0 (C_q, d, $^1J_{C\text{-}F}$== 254 Hz) . ^{19}F (282 MHz, $CDCl_3$, ppm) : -110.16 (Td, J= 14.2, 5.5 Hz) (**Fig. S3**).

2.3. X-ray crystallography of 5-fluoro-benzo[c][2,1,3]selenadiazole (**C2**)

A yellowish crystal of ($C_6H_3FN_2Se$) (**Fig. 1**) was mounted on a Bruker APEX-II CCD duo diffractometer using graphite monochromated Mo Kα radiation (λ= 0.71073Å). The structure was solved by direct method SHELXS-97 and refined by full-matrix least-squares procedures on F^2 [23,24]. XP (Bruker AXS) and Mercury were used for graphical representations [25].

CCDC 1896845 (**C2**) contains the supplementary crystallographic data for this paper. These data are provided free of charge by The Cambridge Crystallographic Data Centre. The details of refinement parameters are given in **Table 1**.

Table 1
Crystallographic and structure refinement parameters for [$C_6H_3FN_2Se$].

Chemical formula	$C_6H_3FN_2Se$
Formula weight	201.06
Crystal system	monoclinic
Space group	$P\ 2_1/c$

Crystal color	yellowish
Radiation type	Mo Kα
a (Å)	13.2549(6)
b (Å)	3.8667(2)
c (Å)	13.0731(6)
β (°)	109.309(2)
V (Å^3)	632.34(5)
Z	4
T (K)	150 (2)
R_{int}	0.0241
Final R indices [I>2σ(I)]*	0.0200, wR_2 0.0517
R indices (all data)	0.0222, wR_2 0.0532

Computer programs: APEX2 (Bruker, 2014), SAINT (Bruker, 2013), SAINT, SHELXS97 (Sheldrick, 2008), SHELXL2014/7(Sheldrick,2015), Mercury (Macrae et al., 2006), publCIF (Westrip, 2010)

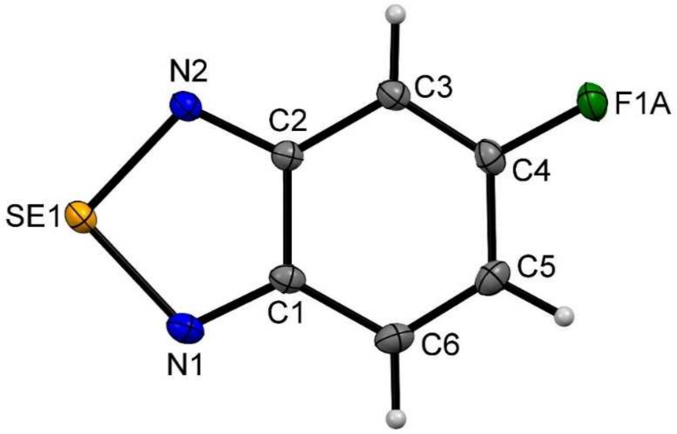

Fig. 1. The molecular structure of **C2** with displacement ellipsoids drawn at the 30% probability level

2.4. Computational studies

All theoretical calculations presented in this paper were performed using the Gaussian 09 program package [26]. The full geometries of **C1** and **C2** were optimized employing DFT method in a vacuum and in 1,4-dioxane as solvent using B3LYP level of theory in conjunction with 6-311G(d.p) basis set, which was assigned for all atoms [27].

Vibrational frequency calculations were computed in order to ensure that the optimized geometries are the most stable (only positive values were obtained). Electronic transitions in the UV absorption spectra based on the optimized geometries were carried out employing TD-DFT approach [28] in 1,4-dioxane as solvent with the conductor like polarizable continuum model (C-PCM) [29]. Gaussum program [30] was used to delineate with the rate contributions of each group to a particular molecular orbital (MO) by means of Natural Bond Orbital (NBO). Thereafter, the Fukui functions were calculated using NBO analysis [31] at DFT/B3LYP level in order to understand the transfer of charges or conjugative interactions in a molecular system.

2.5. Electrochemical study

The cyclic voltammetry (CV) measurements were performed using a potentiostat PGZ100 with a three-electrode configuration. A platinum wire working electrode, a platinum mesh auxiliary electrode and Ag/AgCl (Saturated KCl) reference electrode. All references reported in this manuscript are versus the reference electrode. The CV measurements were achieved in sodium sulfate solution (Na_2SO_4 = 1 M) /1,4-dioxane (90/10: v/v) as the supporting electrolyte (pH=4.53) at 298±1 K with a scanning rate of 50 mV/s. The solutions were deoxygenated with bubbling nitrogen ($N_{2(g)}$) at least 10 min during the electrochemical measurements.

3. Results and discussion

*3.1. Description of the crystal structure of **C2***

The titled compound was prepared in DMF by reacting 4-Fluoro-o-phenylenediamine with selenium dioxide at room temperature as shown in Scheme 1. The ^{1}H NMR spectrum shows only three peacks at 7.3, 7.4 and 7.8 ppm corresponding to the aromatic protons. Furthermore, the single crystal x-ray diffraction analysis of C2 confirmed the assignments of the structure from spectroscopic data. The crystal packing of $C_6H_3FN_2Se$ shows that the molecules are arranged in rods along b axis (**Table 2 and Fig. 2**).

Table 2
Hydrogen-bond geometry (Å, °) for **C2**.

D - H···A	D - H	H···A	D···A	D-H···A
C(3) -H(3) ···N(1)^i	0.95	2.55	3.490(3)	169
C(6) -H(6) ···F(1A)^{ii}	0.95	2.50	3.446(3)	174

Symmetry codes: (i) x,1/2-y,1/2+z; (ii) x,3/2-y,-1/2+z

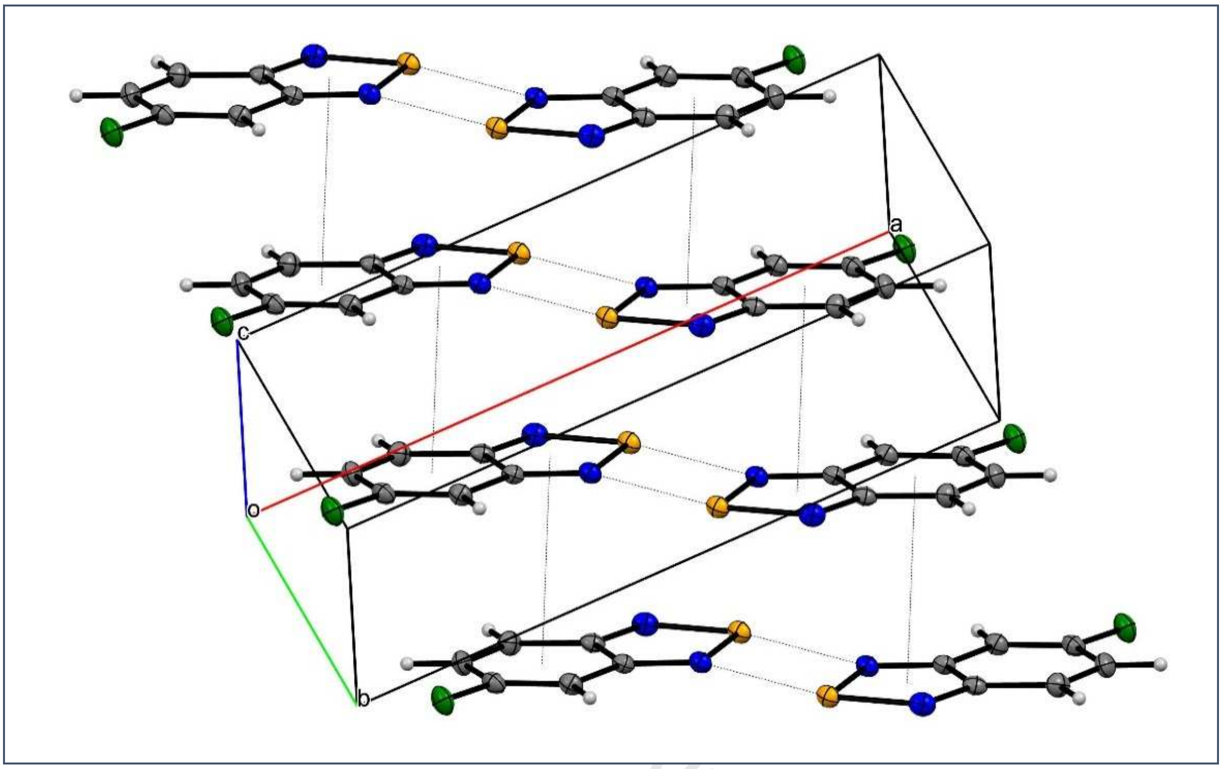

Fig. 2. Part of the packing diagram of **C2**, showing Se···N contacts and π···π stacking interactions as dotted lines. Displacement ellipsoids are drawn at the 30% probability level. For clarity lower occupancy sites are omitted.

The formation of dimeric units by intermolecular Se···N interactions (Se···N2 = 2.853(2) Å) is observed as found for 4,5,6,7-tetramethyl-2,1,3-benzoselenadiazole and their cocrystals [32]. Additionally, π···π stacking interactions are found between the 1,2,5-selenadiazole and the six-membered aromatic ring [centroid–centroid distance = 3.596(2) Å and ring slippage = 1 Å].

3.2. Vibration spectra

The theoretical FT-IR spectra of the titled compounds were calculated at the B3LYP/6-311G(d,p) level of theory. The scaled vibration modes are obtained at the same level of theory and scaled with a factor of 0.9619 [33]. It is observed that the stretching vibration modes of C=N bond for **C1** and **C2** are respectively located at 1493.07 cm^{-1} and 1492.77 cm^{-1} (**Fig. S1**), which are closer to their corresponding scaled ones at 1476.36 cm^{-1} and 1472.45 cm^{-1}. For the N-Se bond, it is observed that the vibrational frequencies at 745.13 cm^{-1} and 750.13 cm^{-1} for **C1** and **C2** are in good agreement with the calculated values, whereas the corresponding scaled ones were found at 720.30 cm^{-1} and 719.86 cm^{-1}, respectively. The main observed vibrational modes and their corresponding computed and scaled ones are given in **Table 3**.

Table 3
Experimental, theoretical and scaled vibrational wavenumbers (cm^{-1}) of the titled compounds at B3LYP/6-311G(d,p) level and their assignments.

	Assignments	Experimental values	Theoretical scaled values
C1	**υ(C=C)**	1623.01	1603.78
	υ(C=N)	1493.07	1476.36
	υ(N-Se)	745.13	720.30
C2	**υ(C=C)**	1621.76	1601.38
	υ(C=N)	1492.77	1472.45
	υ(N-Se)	750.13	719.86

3.3. Computational investigations and DFT modeling

DFT modeling is a powerful and a widely used tool for dealing with the stability, reactivity and selectivity of inorganic and organic molecules. To gain a better understanding of the electronic structure of the titled compounds, the optimization of **C1** and **C2** was carried out in the single ground by DFT method at B3LYP level of theory. The experimental and computed geometrical parameters of **C1** and **C2** are listed in **Table 4**. For both compounds, all computed bond lengths and bond angles are in good agreement with the experimental findings.

Table 4
Experimental and theoretical selected geometry parameters (value Å and degree) for **C1** and **C2** compounds.

	C1				**C2**		
	Calculated		**Experimental**		**Calculated**		**Experimental**
	Gas	**Solvent**			**Gas**	**Solvent**	
Bond (Å)				**Bond (Å)**			
Se-N1	1.807	1.808	1.792 (17)	Se-N1	1.795	1.795	1.794 (19)
Se-N2	1.808	1.808	1.790 (18)	Se-N2	1.794	1.794	1.795 (18)
C1-C6	1.464	1.464	1.453 (3)	C1-C2	1.453	1.453	1.453 (3)
C4-C7	1.507	1.506	1.505 (3)	C4-F	1.345	1.344	1.360 (3)
N1-C1	1.323	1.324	1.332 (3)	N1-C1	1.322	1.322	1.330 (3)
N2-C6	1.324	1.325	1.331 (2)	N2-C2	1.331	1.330	1.322 (3)
Angles (°)				**Angles (°)**			
N1-Se-N2	94.242	94.086	94.54 (8)	N1-Se-N2	93.968	93.968	93.9 (8)
Se-N1-C1	106.231	106.388	106.37 (13)	Se-N1-C1	106.885	106.885	106.7 (14)
Se-N2-C6	106.334	106.488	106.57 (13)	Se-N2-C2	106.732	106.732	106.8 (14)

C7-C4-C3	118.449	118.436	118.44 (17)	F-C4-C5	122.557	122.557	117.4 (2)
C7-C4-C5	121.709	121.733	121.81 (18)	F-C4-C3	116.768	116.768	118.4 (2)

Additionally, contour plot for some selected molecular orbitals (MOs) are presented in **Fig. 3**. The corresponding energies of these MOs as well as the percent composition of each element for the titled compounds are summarized in **Table 5**. The higher energy occupied molecular orbital (HOMO) to the low-lying virtual orbital (LUMO) band gap energies are 3.99 eV and 4.01 eV for **C1** and **C2**, respectively.

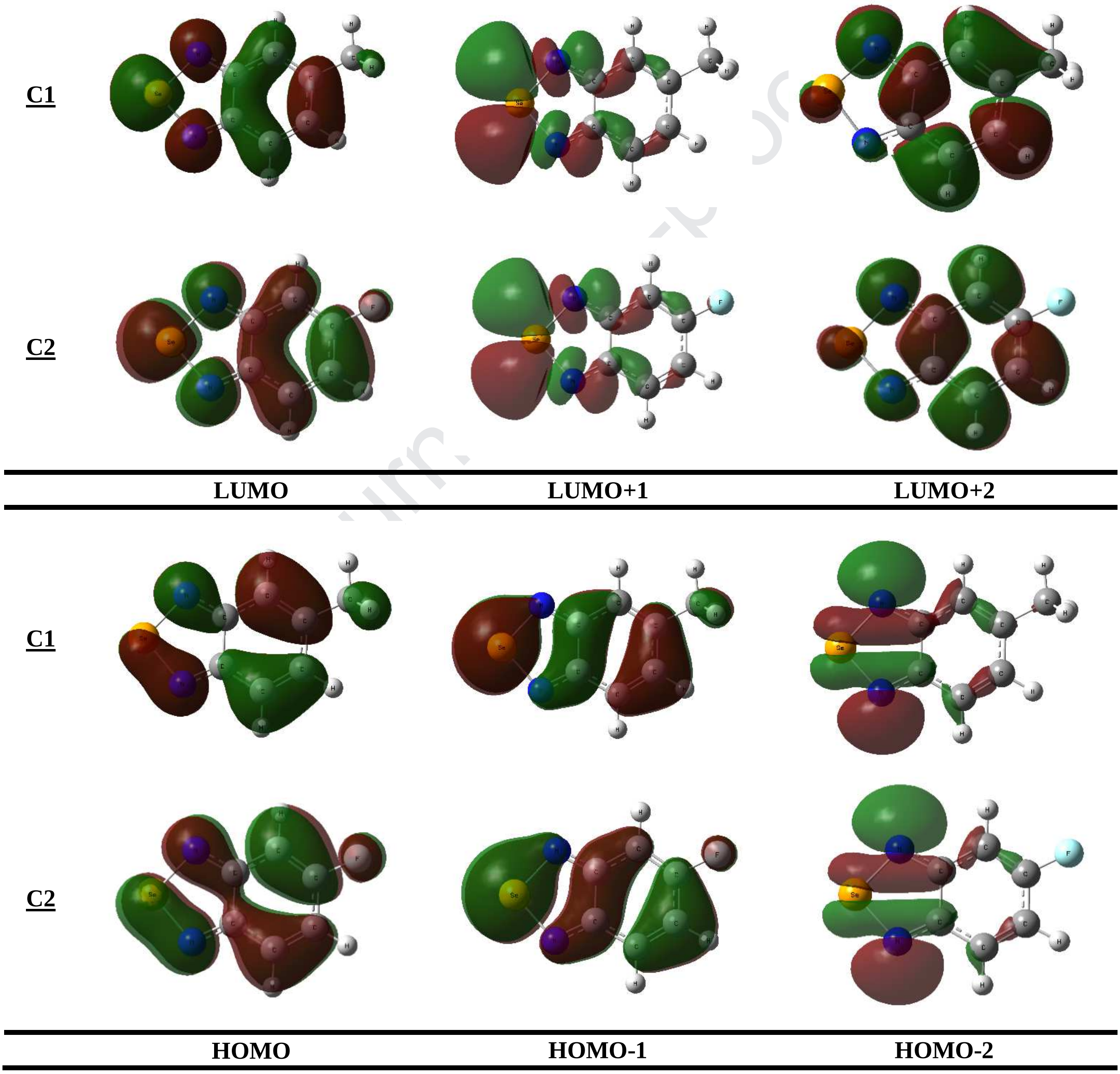

Fig. 3 Isodensity surface plots of the frontier molecular orbitals for **C1** and **C2**.

Table 5
Energy and composition of some selected molecular orbitals (MOs) for **C1** and **C2**.

		% of composition in **C1**				% of composition in **C2**		
MOs	Energy (eV)	Se	CH_3	L	Energy (eV)	Se	F	L
LUMO+3	0.12	2	5	93	0.09	2	2	96
LUMO+2	-0.01	2	2	96	-0.27	2	0	98
LUMO+1	-0.77	81	0	19	-0.90	80	0	19
LUMO	-2.58	20	1	79	-2.80	21	1	78
HOMO	-6.57	3	3	95	-6.81	5	4	90
HOMO-1	-6.97	46	2	53	-7.20	43	1	56
HOMO-2	-8.08	7	0	93	-8.33	6	0	94
HOMO-3	-8.40	18	1	81	-8.72	19	0	80

3.4. TD-DFT calculations and electronic spectrum

For both compounds **C1** and **C2** along with the used reagents **1** and **2**, the UV absorption spectra have been performed using 1,4-dioxane as solvent in the range of 200-900 nm. The experimental spectra for **C1** and **C2** are shown in **Fig. 4** and the corresponding spectra of **1** and **2** are given in supporting information **(Fig. S5**). For the compounds **1** and **2**, we observed similar absorption bands at 245 nm and 305 nm with a slight difference in their intensity. This difference is due to the auxochrome effect caused by the fluorine atom in **2**. Whereas, in the UV region for **C1** and **C2**, all absorption bands are slightly superimposed until the wavelength 335 nm, where **C2** above slightly **C1** in terms of absorption band and wavelength. These results indicate the hyperchromic effect exhibited by the fluorine auxochrome in **C2** which leads to an increase of absorption maxima because of the n-π^* conjugation. Moreover, from 200 nm to 266 nm we have noticed that **SeO_2**, **C1** and **C2** show the same band shape. These compounds exhibit the same band at 244 nm and differ in terms of intensity. While, there is no significant absorption in the visible region (400-800).

Therefore, to study the nature of the excitations in the UV spectra, the absorption bands of **C1** and **C2** were carried out by TD-DFT method using 1,4-dioxane as solvent. The experimental bands with the computed excitation energies, absorption bands, oscillator strengths and MOs transition configurations are summarized in **Table 6**. As can be seen from this table, the electronic transitions shown at 354 nm (f = 0.0458) and 350 nm (f = 0.0577) correspond to HOMO → LUMO transitions (97% for **C1** and 96% for **C2**), with ligand to selenium charge transfer character (**LSeCT**) for **C1** and **C2**, respectively.

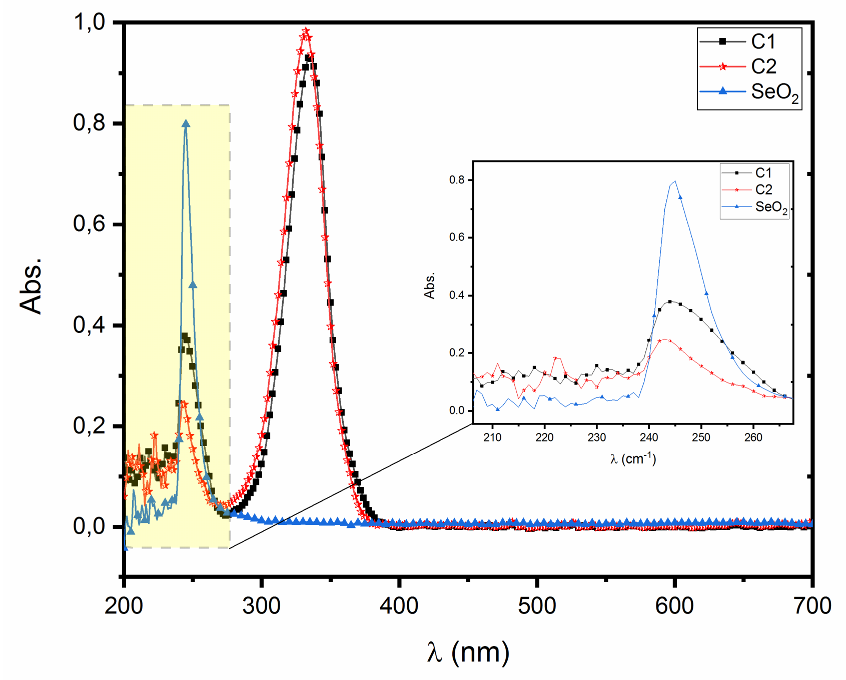

Fig. 4. Experimental UV-vis spectrum for **SeO$_2$**, **C1** and **C2** in 1,4-dioxane.

Table 6
Experimental and calculated electronic transitions by TDDFT/C-PCM method for **C1** and **C2** in 1.4-dioxane.

	E_e (eV)	λexp. (nm)	λ_e (nm)	Osc. Strength (f)	Key transitions	Character
C1	3.504802	335	354	0.0458	HOMO → LUMO (97%)	**LSeCT**, Pπ (L) → Pπ (Se)
	4.041402	-	307	0.3364	H-1 → LUMO (94%)	**SeLCT**, Pπ (Se) → Pπ (L)
	4.263602	-	291	0.0000	H–2 → LUMO (99%)	**LSeCT**, Pπ (L) → Pπ (Se)
	4.905303	-	252	0.0009	HOMO → L+1 (92%)	**LSeCT**, Pπ (L) → Pπ (Se)
	5.069803	244	244	0.0002	H–1 → L+1 (93%)	**LSeCT**, Pπ (L) → Pπ (Se)
C2	3.541302	332	350	0.0577	HOMO → LUMO (96%)	**LSeCT**, Pπ (L) → Pπ (Se)
	4.070402	-	305	0.3125	H–1 → LUMO (93%)	**SeLCT**, Pπ (Se) → Pπ (L)
	4.234502	-	293	0.0000	H–2 → LUMO (99%)	**LSeCT**, Pπ (L) → Pπ (Se)
	4.943403	-	250	0.0005	HOMO → L+1 (89%)	**LSeCT**, Pπ (L) → Pπ (Se)
	5.172503	243	240	0.0004	H–1 → L+1 (91%)	**LSeCT**, Pπ (L) → Pπ (Se)

3.5. Fukui functions

Fukui function, the most commonly applied local reactivity parameter, is defined as the derivative of electron density with respect to the charge in the number of electrons density keeping the positions of the nuclei remaining unaltered [34,35]. Fukui indices give information about electrophilic/nucleophilic power of such atomic site in a molecular system.

In order to quantify the tendency of each atom in a molecule with a numerical value to indicate its ability to serve as a reactive site, condensed Fukui functions are investigated. The condensed Fukui functions on the Kth atom site are represented as:

$$f^{+}_{k} = q_k\,(N+1) - q_k\,(N) \qquad (1)$$

$$f^{-}_{k} = q_k\,(N) - q_k\,(N-1) \qquad (2)$$

$$\Delta f(r) = f^{+}_{k} - f^{-}_{k} \qquad (3)$$

Where, f^{+}_{k} for nucleophilic attack and f^{-}_{k} for electrophilic attack. In these equations, q_k is the atomic charge at the kth atomic site in the neutral (N), anionic (N+1) or cationic (N-1) chemical species. In the present study, the values of Fukui function were calculated from NBO charges. Morrel et al. [36] have proposed a new dual descriptor $\Delta f(r)$ for the calculation of nucleophilicity and electrophilicity and is defined as the difference between the nucleophilic and electrophilic Fukui function. If $\Delta f(r) > 0$, the site is prone for nucleophilic attack, while the site is apt to electrophilic attack when $\Delta f(r) < 0$. The condensed Fukui functions (f^{+}_{k}), (f^{+}_{k}) and dual descriptor $\Delta f(r)$ are given in **Table 7**. In the present work, we found that Se atom in **C1** is prone to nucleophilic attack as it has $\Delta f(r) > 0$ whereas Se in **C2** is prone for electrophilic attack as it has $\Delta f(r) < 0$. The such result could be related to the nature of the substituent.

Table 7

Fukui indices for nucleophilic and electrophilic sites on atoms computed form natural bond orbital analysis at DFT/6-311G(d.p) in 1,4-dioxane.

	C1				**C2**		
Atom	f^{+}_{k}	f^{-}_{k}	$\Delta f(r)$	Atom	f^{+}_{k}	f^{-}_{k}	$\Delta f(r)$
C	0.0512	-0.0262	0.0773	C	0.0447	-0.0172	0.0619
C	0.0235	-0.0301	0.0535	C	0.0116	-0.0329	0.0445
C	-0.1945	-0.0721	-0.1224	C	-0.1737	-0.0768	-0.0969
H	-0.0269	-0.0317	0.0048	H	-0.0280	-0.0324	0.0044
C	0.0035	-0.0764	0.0799	C	0.0065	-0.0931	0.0995
H	-0.0354	-0.0286	-0.0068	H	-0.0367	-0.0289	-0.0078
C	-0.1112	-0.0666	-0.0446	C	-0.1046	-0.0474	-0.0573
C	-0.2094	-0.0649	-0.1444	C	-0.2024	-0.0725	-0.1299
H	-0.0276	-0.0308	0.0032	H	-0.0292	-0.0315	0.0023
N	-0.1055	-0.1022	-0.0033	N	1.6273	-0.0988	1.7261
N	-0.1100	-0.1043	-0.0057	N	-0.0956	-0.1039	0.0082
Se	-0.1793	-0.3139	0.1346	Se	-25.5706	-0.3217	-25.2488
C	0.0253	0.0119	0.0134	F	23.5509	-0.0428	23.5937
H	-0.0398	-0.0234	-0.0165				
H	-0.0440	-0.0172	-0.0269				

H	-0.0199	-0.0238	0.0039

3.6. *Electrochemical studies*

Electrochemical analysis focuses in phenomena resulting from combined electrical and chemical effects. In our study, we used CV as a useful technique to investigate the electrochemical behavior such as redox process, stability of reaction products, adsorption processes and the presence of intermediates in redox reactions of considered compounds. [37]. The influence of different groups (R = CH_3, F) on the redox potential was assessed using CV. **Fig. 5** shows the investigation of **SeO_2**, **C1** and **C2** in Na_2SO_4 (1M)/1,4-dioxane electrolyte solution within potential range of -1.0 V to 1.5 V at 50 mV/s scan rate. The electrochemical parameters are gathered in **Table 8**.

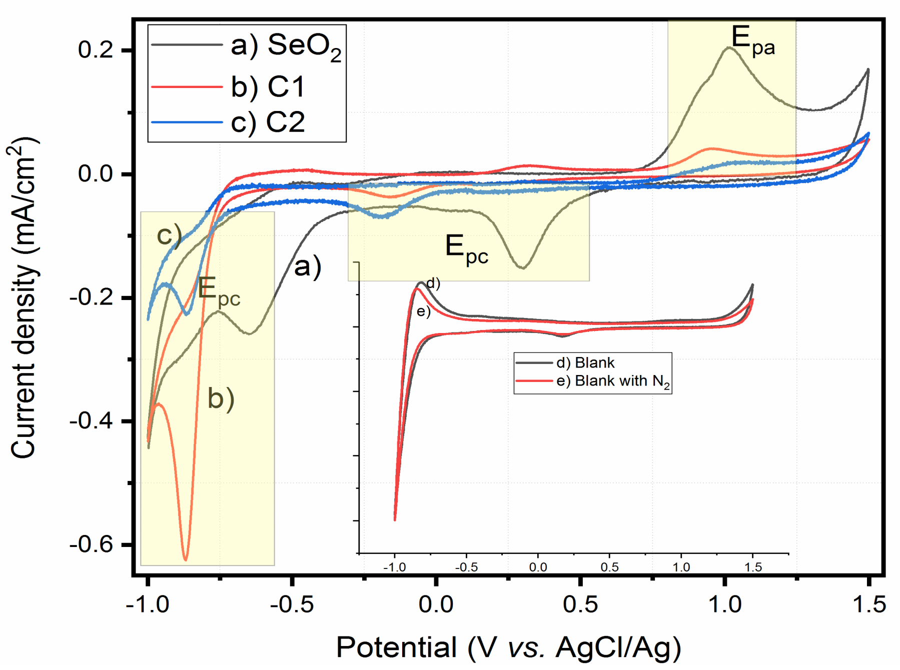

Fig. 5. Cyclic voltammograms of **SeO_2**, **C1** and **C2** in Na_2SO_4/1,4-dioxane (90/10) (v/v).

Table 8

Electrochemical parameters obtained for **SeO_2**, **C1** and **C2** at 50 mV s^{-1} scan rate.

	E_{pa} (V)	E_{pc} (V)
SeO_2	1.012	0.296
	0.149	-0.652
C1	1.012	-0.161
	0.315	-0.870
C2	1.06	-0.196
	0.317	-0.863

The comparison of the electrochemical behavior of both compounds with **SeO_2** shows that they exhibit the same anodic behavior (E_{pa}) for the redox potential. Whereas, the cathodic behavior (E_{pc}) for **C1** and **C2** shifts to negative values of the potential comparing to the one associated to **SeO_2** curve. The peaks at the potential 0.296 V, -0.161 V, -0.196 V and at -0.652 V, -0.870 V, -0.863 V, respectively for **SeO_2, C1** and **C2** are due to the reduction of Se(IV) [38]. The pH value of the solution was 4.53 and the **SeO_2** is in the form of selenious acid ($HSeO_3^-$) [39]. As described in the literature, the reaction mechanism that seems be occur was the reduction of Se(IV) to Se(s) followed by the reduction of Se(s) to H_2Se [40–42]:

$$HSeO_3^- + 5H^+ + 4e^- \leftrightharpoons Se_{(s)} + 3H_2O \quad (4)$$

$$Se_{(s)} + 2H^+ + 2e^- \leftrightharpoons H_2Se_{(aq)} \quad (5)$$

Below -1.0 V, hydrogen evolution begins. The response of the peaks occurring at 0.149, 0.315, 0.317 V and at 1.012, 1.012, 1.06 V respectively for **SeO_2, C1** and **C2** results from the oxidation of the compounds [41]. Under these observations, it is clear that the electrochemical oxidation of the compounds (**C1** and **C2**) have become well separated comparing to the peak of **SeO_2** (**Table 8**) [43].

Furthermore, based on cyclic voltammograms curves (**Fig. 5**), we have noticed that the intensity in current density of **C2** is lower and inhibited than the one of **C1**. This result could be explained by the electronic effect of the Fluorine atom in **C2**. Also, this behavior is observed from the computed Fukui indices (Δ *f*(r) of 23.59 for ***F*** atom) compared to **C1** with a methyl moiety (Δ *f*(r) of 0.01 for ***CH_3*** group). In addition, for **C2**, Fluorine atom as the most electronegative element, its effect on selenium is clearly observed in terms of reactivity. For this reason, this behavior is shown in the redox process of **C2** (see **Fig. 5**). The obtained cyclic voltammograms show clearly that both molecules exhibit an irreversible redox process.

3.7. *Optical and electrochemical properties*

The UV-visible absorption spectra and CV curve of studied compounds were recorded in order to study the optical proprieties and molecular orbital energy levels as shown in **Fig. 4** and **Fig. 5**. The maximal absorption wavelength (λ_{max}) and onset wavelength (λ_0) values and oxidation/reduction potentials determined from the onset of the cyclic voltammograms are reported in **Table 9**.

Difference of energy levels (E_g) between the LUMO and HOMO were determined using the onset wavelength [44,45]:

$$E_g = \frac{hc}{\lambda_0} \qquad (6)$$

h is Plank's constant (h= 6.626 × 10^{-34} J·s); c is the speed of light (3× 10^{8} m/s); and λ_o is the onset wavelength (nm).

The LUMO energy level values of the acceptors for **SeO$_2$** and the studied compounds (**C1** and **C2**) relative to ferrocene/ferrocenium ($E_{Fc^+/Fc}$) as an internal standard, were estimated using the oxidation potential onset:

$$E_{LUMO} = -e\left(E_{red}^{onset} + E_{Fc^+/Fc}\right) = -e\left(E_{red}^{onset} + 4.85\right) \qquad (7)$$

Whereas the values of HOMO energy level were calculated using the following equation:

$$E_{HOMO} = \left(E_{LUMO} - E_g\right) \qquad (8)$$

Table 9
Optical and electrochemical properties **SeO$_2$**, **C1** and **C2**.

Compound	$\lambda(abs)_{max}$/nm	λ_0/nm	E_g (eV)	E_{ox}^{onset} (V)	E_{red}^{onset} (V)	E_{LUMO} (eV)	E_{HOMO} (eV)	ΔE Theoretical/(eV)
SeO$_2$	245	272	4.57	0.759	-0.380	-4.470	-9.320	--
C1	334	378	3,29	0.796	-0.723	-4.127	-8.977	3.99
C2	332	369	3,37	0.730	-0.767	-4.083	-8.933	4.01

Table 9 summarizes the oxidation and the reduction of the onset potentials for the studied products. It is clear that the onset of oxidation process for the compounds **C1** and **C2** is almost closer (0.796 V and 0.730 V) to each other. The same observation was observed for

the onset of reduction (-0.723 V and -0.767 V). HOMO energy level of **C1** (-8.977 eV) is slightly lower than the one of **C2** (-8.933 eV). Hence, a functional methyl group of the **C1** compared to a Fluorine atom of **C2** showed exceedingly a reduction of the bandgap values of **3.29** and **3.37** eV**,** respectively. This observation is confirmed by theoretical finding (Δ**E** $_{\text{Theoretical}}$). As a result, this reduction is due to the electron-donating of Fluorine atom which increase the conjugation and delocalization in the compound [46]. These results indicate the chemical stability of the titled compounds.

4. Conclusion

This research focuses on the synthesis, computational and electrochemical behavior of two benzo[c][1,2,5]selenadiazole organoselenium derivatives. The structures of the studied products (**C1** and **C2**) were fully characterized by FT-IR, ^{1}H NMR, ^{13}C NMR ^{19}F NMR UV visible and Ms-EI. The single crystal analysis shows that each product crystallizes in monoclinic system with P2/c space group. The optimized geometrical parameters (bond lengths, bond angles) were theoretically calculated by DFT method and compared with the experimental values showing a good agreement for both components. The electronic transitions are also estimated by employing TD-DFT theory and compared with the experimental UV-Vis spectra. Fukui indices (f+k, f-k) and dual descriptor Δf(r) for Selenium atom present in both molecules indicated that this atom in **C1** is prone to nucleophilic attack, whereas Se atom in **C2** is prone to electrophilic attack. Furthermore, based on CV curves, it has been shown that both molecules exhibit a good solubility and reactivity with an irreversible electrochemical behavior. From CV and UV-Vis curves, the acquired experimental HOMO and LUMO energy level values along with the bandgap energy was found in good agreement with the theoretical findings which confirm the chemical stability of the titled compounds. These results are very promising for investigating the semiconducting properties of the studied products in the photovoltaic devices.

Acknowledgement

The authors are grateful to Ms Anke Spannenberg at the Leibniz-Institut für Katalyse for her help in obtaining the X-ray analysis.

References

[1] A. Pop, A. Silvestru, Organoselenium compounds with N,C,N pincer groups. Synthesis, structure and reactivity, Polyhedron. (2018). doi:10.1016/j.poly.2018.12.041.

[2] M. Karthika, L. Senthilkumar, R. Kanakaraju, Hydrogen-bond interactions in hydrated 6-selenoguanine tautomers: a theoretical study, Struct. Chem. 25 (2014) 197–213. doi:10.1007/s11224-013-0239-8.

[3] S. Panda, A. Panda, S.S. Zade, Organoselenium compounds as fluorescent probes, Coord. Chem. Rev. 300 (2015) 86–100. doi:10.1016/J.CCR.2015.04.006.

[4] D. Plano, E. Ibáñez, J.A. Palop, C. Sanmartín, Synthesis, characterization, crystal structure and cytotoxicity of 2,4-bis(selenomethyl)quinazoline, Struct. Chem. 22 (2011) 1233–1240. doi:10.1007/s11224-011-9816-x.

[5] A. Breder, S. Ortgies, Recent developments in sulfur- and selenium-catalyzed oxidative and isohypsic functionalization reactions of alkenes, Tetrahedron Lett. 56 (2015) 2843–2852. doi:10.1016/j.tetlet.2015.04.045.

[6] G. Mugesh, H.B. Singh, Synthetic organoselenium compounds as antioxidants: glutathione peroxidase activity, Chem. Soc. Rev. 29 (2000) 347–357. doi:10.1039/a908114c.

[7] L. Engman, I. Cotgreave, M. Angulo, C.W. Taylor, G.D. Paine-Murrieta, G. Powis, Diaryl chalcogenides as selective inhibitors of thioredoxin reductase and potential antitumor agents., Anticancer Res. 17 (1997) 4599–605.

[8] C.W. Nogueira, E.B. Quinhones, E.A.C. Jung, G. Zeni, J.B.T. Rocha, Anti-inflammatory and antinociceptive activity of diphenyl diselenide, Inflamm. Res. 52 (2003) 56–63. doi:10.1007/s000110300001.

[9] M. Bień, B. Błaszczyk, K. Kalinowska, J. Młochowski, A.D. Inglot, Antifungal activity of 2-(4-chlorophenyl)-1,2-benzisoselenazol-3(2H)-one, the analog of Ebselen., Arch. Immunol. Ther. Exp. (Warsz). 47 (1999) 185–93.

[10] E. V. Ratushnaya, Y.I. Kirova, M.A. Suchkov, B.I. Drevko, V.B. Borodulin, Synthesis and Antibacterial Activity of Organoselenium Compounds, Pharm. Chem. J. 36 (2002) 652–653. doi:10.1023/A:1023405611793.

[11] H. Wójtowicz, K. Kloc, I. Maliszewska, J. Młochowski, M. Piętka, E. Piasecki, Azaanalogues of ebselen as antimicrobial and antiviral agents: synthesis and properties, Farm. 59 (2004) 863–868. doi:10.1016/j.farmac.2004.07.003.

[12] A.S. Hodage, C. Parashiva Prabhu, P.P. Phadnis, A. Wadawale, K.I. Priyadarsini, V.K. Jain, Synthesis, characterization, structures and GPx mimicking activity of pyridyl and pyrimidyl based organoselenium compounds, J. Organomet. Chem. 720 (2012) 19–25. doi:10.1016/j.jorganchem.2012.08.035.

[13] J.M. HARKIN, A. DONG, G. CHESTERS, Elevation of selenium levels in air by xerography, Nature. 259 (1976) 204–205. doi:10.1038/259204b0.

[14] A. Sahu, L. Qi, M.S. Kang, D. Deng, D.J. Norris, Facile Synthesis of Silver Chalcogenide (Ag 2 E; E = Se, S, Te) Semiconductor Nanocrystals, J. Am. Chem. Soc. 133 (2011) 6509–6512. doi:10.1021/ja200012e.

[15] C.W. Nogueira, G. Zeni, J.B.T. Rocha, Organoselenium and Organotellurium Compounds: Toxicology and Pharmacology, Chem. Rev. 104 (2004) 6255–6286. doi:10.1021/cr0406559.

[16] J. Mochowski, Developments in the chemistry of selenaheterocyclic compounds of practical importance, Phosphorus, Sulfur Silicon Relat. Elem. 183 (2008) 931–938. doi:10.1080/10426500801898408.

[17] M.A. Goodman, M.R. Detty, Selenoxides as Catalysts for the Activation of Hydrogen Peroxide. Bromination of Organic Substrates with Sodium Bromide and Hydrogen Peroxide, Organometallics. 23 (2004) 3016–3020. doi:10.1021/om049908e.

[18] S.R. Mellegaard-Waetzig, C. Wang, J.A. Tunge, Selenium-catalyzed oxidative halogenation, Tetrahedron. 62 (2006) 7191–7198. doi:10.1016/j.tet.2005.12.072.

[19] R.S. Kumar, K. Kulangiappar, M.A. Kulandainathan, Convenient Electrochemical Method for the Synthesis of α-Bromo Alkyl Aryl Ketones, Synth. Commun. 40 (2010) 1736–1742. doi:10.1080/00397910903161710.

[20] A. Hasnaoui, I. Hdoufane, R. Idouhli, B. Therrien, M. Ait Ali, L. El Firdoussi, Crystal structure of {N-(2-hydroxyethylamino) ethylsalicylaldiminato]-palladium(II) chloride}: Synthesis, X-ray structure, electrochemistry, DFT and TDDFT studies, J. Mol. Struct. 1176 (2019) 703–710. doi:10.1016/j.molstruc.2018.08.111.

[21] Y. Wang, Y. Bai, M. Liang, W. Zheng, Differential Pulse Voltammetric Determination of Selenocystine and Selenomethionine Using SAM nanoSe 0 /Vc/SeCys-Film Modified Au Electrode, Electroanalysis. 21 (2009) 2145–2152. doi:10.1002/elan.200804649.

[22] H. Ouahine, M. Ait Ali, L. El Firdoussi, A. Spannenberg, 5-Methylbenzo[d][2,1,3]selenadiazole, IUCrData. 2 (2017) x170226. doi:10.1107/S2414314617002267.

[23] G.M. Sheldrick, Crystal structure refinement with SHELXL, Acta Crystallogr. Sect. C Struct. Chem. 71 (2015) 3–8. doi:10.1107/S2053229614024218.

[24] G.M. Sheldrick, A short history of SHELX, Acta Crystallogr. Sect. A Found. Crystallogr. 64 (2008) 112–122. doi:10.1107/S0108767307043930.

[25] C.F. Macrae, P.R. Edgington, P. McCabe, E. Pidcock, G.P. Shields, R. Taylor, M. Towler, J. Van De Streek, Mercury: Visualization and analysis of crystal structures, J. Appl. Crystallogr. 39 (2006) 453–457. doi:10.1107/S002188980600731X.

[26] M.J. Frisch, G.W. Trucks, H.B. Schlegel, G.E. Scuseria, M.A. Robb, J.R. Cheeseman,

G. Scalmani, V. Barone, B. Mennucci, G.A. Petersson, H. Nakatsuji, M. Caricato, H.P.H. X. Li, A.F. Izmaylov, J. Bloino, G. Zheng, J.L. Sonnenberg, M. Hada, M. Ehara, K. Toyota, R. Fukuda, J. Hasegawa, M. Ishida, T. Nakajima, Y. Honda, O. Kitao, H. Nakai, T. Vreven, J.A.M. Jr., J.E. Peralta, F. Ogliaro, M. Bearpark, J.J. Heyd, E. Brothers, K.N. Kudin, V.N. Staroverov, R. Kobayashi, Normand, J.R. Rendell, K.A.J.C. Burant, S.S. Iyengar, J. Tomasi, M. Cossi, N. Rega, J.M. Millam, M. Klene, J.E. Knox, J.B. Cross, V. Bakken, C. Adamo, J. Jaramillo, R. Gomperts, R.E. Stratmann, O. Yazyev, A.J. Austin, R. Cammi, C. Pomelli, J.W. Ochterski, R.L. Martin, K. Morokuma, V.G. Zakrzewski, G.A. Voth, P. Salvador, J.J. Dannenberg, S. Dapprich, A.D.D.O. Farkas, J.B. Foresman, J.V. Ortiz, J. Cioslowski, D.J. Fox, Gaussian 09, Wallingford CT, (2009). http://gaussian.com/.

[27] A.D. Becke, Density-functional thermochemistry. III. The role of exact exchange, J. Chem. Phys. 98 (1993) 5648–5652. doi:10.1063/1.464913.

[28] R.E. Stratmann, G.E. Scuseria, M.J. Frisch, An efficient implementation of time-dependent density-functional theory for the calculation of excitation energies of large molecules, J. Chem. Phys. 109 (1998) 8218–8224. doi:10.1063/1.477483.

[29] M. Cossi, N. Rega, G. Scalmani, V. Barone, Energies, structures, and electronic properties of molecules in solution with the C-PCM solvation model, J. Comput. Chem. 24 (2003) 669–681. doi:10.1002/jcc.10189.

[30] N.M. O'boyle, A.L. Tenderholt, K.M. Langner, cclib: A library for package-independent computational chemistry algorithms, J. Comput. Chem. 29 (2008) 839–845. doi:10.1002/jcc.20823.

[31] A.E. Reed, L.A. Curtiss, F. Weinhold, Intermolecular interactions from a natural bond orbital, donor-acceptor viewpoint, Chem. Rev. 88 (1988) 899–926. doi:10.1021/cr00088a005.

[32] K. Eichstaedt, A. Wasilewska, B. Wicher, M. Gdaniec, T. Połoński, Supramolecular Synthesis Based on a Combination of Se···N Secondary Bonding Interactions with Hydrogen and Halogen Bonds, Cryst. Growth Des. 16 (2016) 1282–1293. doi:10.1021/acs.cgd.5b01356.

[33] M.P. Andersson, P. Uvdal, New Scale Factors for Harmonic Vibrational Frequencies Using the B3LYP Density Functional Method with the Triple-ζ Basis Set 6-311+G(d,p), J. Phys. Chem. A. 109 (2005) 2937–2941. doi:10.1021/jp045733a.

[34] W. Yang, W.J. Mortier, The use of global and local molecular parameters for the analysis of the gas-phase basicity of amines, J. Am. Chem. Soc. 108 (1986) 5708–5711. doi:10.1021/ja00279a008.

[35] P.W. Ayers, R.G. Parr, Variational Principles for Describing Chemical Reactions: The Fukui Function and Chemical Hardness Revisited, J. Am. Chem. Soc. 122 (2000) 2010–2018. doi:10.1021/ja9924039.

[36] C. Morell, A. Grand, A. Toro-Labbé, Theoretical support for using the Δf(r) descriptor, Chem. Phys. Lett. 425 (2006) 342–346. doi:10.1016/j.cplett.2006.05.003.

[37] J. David K. Gosser, Cyclic Voltammetry; Simulation and Analysis of Reaction Mechanisms, 1994. doi:10.1080/00945719408001398.

[38] S. Zein El Abedin, A.Y. Saad, H.K. Farag, N. Borisenko, Q.X. Liu, F. Endres, Electrodeposition of selenium, indium and copper in an air- and water-stable ionic liquid at variable temperatures, Electrochim. Acta. 52 (2007) 2746–2754. doi:10.1016/j.electacta.2006.08.064.

[39] M. Bouroushian, Electrochemistry of the Chalcogens, in: 2010: pp. 57–75. doi:10.1007/978-3-642-03967-6_2.

[40] M.F. Cabral, V.A. Pedrosa, S.A.S. Machado, Deposition of selenium thin layers on gold surfaces from sulphuric acid media: Studies using electrochemical quartz crystal microbalance, cyclic voltammetry and AFM, Electrochim. Acta. 55 (2010) 1184–1192. doi:10.1016/j.electacta.2009.10.008.

[41] R. Chen, D. Xu, G. Guo, Y. Tang, Electrodeposition of silver selenide thin films from aqueous solutions, J. Mater. Chem. 12 (2002) 1437–1441. doi:10.1039/b107177g.

[42] M.C. Santos, S.A.S. Machado, Microgravimetric, rotating ring-disc and voltammetric studies of the underpotential deposition of selenium on polycrystalline platinum electrodes, J. Electroanal. Chem. 567 (2004) 203–210. doi:10.1016/j.jelechem.2003.12.026.

[43] G. Jarzabek, Z. Kublik, Determination of traces of selenium(IV) by cathodic stripping voltammetry at the hanging mercury drop electrode, Anal. Chim. Acta. 143 (1982) 121–130. doi:10.1016/S0003-2670(01)95492-3.

[44] Y.-F. Zhang, C.-Z. Zhang, Experimental and theoretical study on spontaneous intermolecular charge transfer features and antiaromaticities of unusual bisazo compounds with antiaromatic cores, J. Mol. Struct. 1189 (2019) 225–232. doi:10.1016/j.molstruc.2019.04.044.

[45] Y. Zhang, F. Wu, Synthesis of a new W-type of functional polymer for improving intermolecular charge transfer processes at donor/acceptor interfaces, High Perform. Polym. 31 (2019) 521–527. doi:10.1177/0954008319827066.

[46] C.-Z. Zhang, D. Shen, Y. Yuan, S.-J. Li, H. Cao, Syntheses and Optoelectronic Properties of Planar Compounds 3,7-diaryl-1,5,2,4,6,8-dithiotetrazocine, J. Heterocycl. Chem. 53 (2016) 1813–1819. doi:10.1002/jhet.2491.

Highlight

-Two benzo[1,2,5]selenadiazoles have been synthesized and characterized by different spectroscopic techniques.

-The structures of both components have been confirmed by single crystal X-ray analysis

-The geometrical parameters, electronic transitions, fukui indices and redox properties the molecules have been interpreted by DFT and TDDFT calculations.

-Cyclic voltammograms show that the both compounds exhibit an irreversible redox process.